Microporous and Mesoporous Materials 174 (2013) 100–107

Contents lists available at SciVerse ScienceDirect

Microporous and Mesoporous Materials

journal homepage: www.elsevier.com/locate/micromeso

Selective detection of olefins using a luminescent silver-functionalized metal organic framework, RPM3

Anne M. Marti [a], Nour Nijem [b], Yves J. Chabal [a,b], Kenneth J. Balkus Jr. [a,*]

[a] Department of Chemistry and the Alan G. MacDiarmid Nanotech Institute, 800 West Campbell Rd., University of Texas at Dallas, Richardson, TX 75080, United States
[b] Laboratory for Surface and Nanostructure Modification, Department of Material Science and Engineering, 800 West Campbell Rd., University of Texas at Dallas, Richardson, TX 75080, United States

ARTICLE INFO

Article history:
Received 23 December 2012
Received in revised form 8 February 2013
Accepted 28 February 2013
Available online 14 March 2013

Keywords:
Metal organic framework (MOF)
RPM3
π Complex
Olefin/paraffin separations
Olefin sensor

ABSTRACT

A highly flexible, luminescent, three-dimensional metal organic framework (MOF), $[Zn_2(bpdc)_2(bpee)]\cdot 2DMF$ (bpdc = 4,4′-biphenyldicarboxylate; bpee = 1,2-bipyridylethylene) also known as RPM3 was post functionalized with $AgNO_3$ forming a π complex with the MOF's conjugated linkers. The Ag^+ functionalized MOF in its activated form exhibits structural rearrangements from the interaction of Ag^+ ions monitored by Raman spectroscopy. The reversible binding of olefins such as ethylene (C_2H_4) and 1-hexene (C_6H_{12}) by the Ag^+ functionalized MOF was monitored by fluorescence and Raman spectroscopy. These findings hold promise for the utilization of RPM3 for olefin/paraffin based separations and for a MOF based chemical sensor applicable for the detection of olefins.

1. Introduction

Light olefin (C_nH_{2n}) production is in high worldwide demand due to their role in the fabrication of daily used products such as plastics, fibers, and other chemicals. Typically olefins are produced from steam cracking processes where light olefins are converted from hydrocarbon feedstocks; this process is very expensive and energy intensive. Cryogenic distillation is then used to separate the olefins produced from their corresponding paraffins. The distillation process is also expensive and energy intensive due to the small separation factor between olefin/paraffins. Therefore, alternative separation processes such as reactive adsorption have been under investigation in order to reduce costs [1,2]. New adsorption studies are primarily focused on developing new materials that can selectively adsorb one hydrocarbon over another. Some examples are porous solids [3], adsorbents functionalized with Ag and Cu such as zeolites [4,5], ionic liquids [6,7], polymers [8], and liquid gas membrane contactors [9].

Olefins such as ethylene (C_2H_4) are important for the manufacturing of chemicals including polymers [10]. The separation and detection of ethylene is a challenge that impacts not only the chemical industry but also environmental, agricultural, and medical fields. Environmentally, ethylene is considered a precursor pollutant of which is produced from the combustion from furnaces. It is involved within the generation of tropospheric ozone present in smog, which can cause health problems such as respiratory irritation and cardiovascular effects [10,11]. It has also been reported that ethylene is present within the human breath of patients going through radiotherapy. Ionizing radiations (X-rays) used in radiotherapy produce free radicals that cause cell damage and cell death; these free radicals induce lipid peroxidation in lung epithelium. Lipid peroxidation is the oxidative degradation of fatty acids induced by free radicals; thus ethylene is produced from the degradation of the fatty acid, linolenic acid. Ethylene gas is not metabolized by the body, but diffuses rapidly into the bloodstream and is exhaled in the breath. As a result, ethylene has been of interest in the pharmaceutical industry as a detectable biomarker to monitor the progress of radiotherapy without inducing harm or discomfort to the patient [12]. Ethylene is also of great importance to the horticultural industry as well; since it is a plant hormone involved in many physiological processes such as the ripening and senescence of vegetables, fruits, and flowers [13,14] At concentrations >20 ppm, ethylene starts to affect the shelf life of produce; therefore many methods to monitor ethylene concentration levels have been developed [15]. Current ethylene detection is accomplished using laser acoustic techniques [11,16] gas chromatography [17] and electrochemical and or optical sensors of which have a wide dynamic range of detection from the ppb to ppm concentrations [18]. However current detection methods can become costly due to their large complex systems or costly electrode materials, hence the generation of a small scale, cost effective system would be beneficial.

Metal–organic frameworks (MOFs) are a relatively new class of porous crystalline materials that continue to grow in interest [19].

* Corresponding author. Tel.: +1 972 883 2659; fax: +1 972 883 2925.
E-mail address: balkus@utdallas.edu (K.J. Balkus Jr.).

1387-1811/$ - see front matter © 2013 Elsevier Inc. All rights reserved.
http://dx.doi.org/10.1016/j.micromeso.2013.02.044

MOF structures are composed of inorganic metal ions and organic linkers that combine to form hybrid porous materials with exceptionally high surface areas [20,21]. Many MOFs then maintain porosity upon the removal of solvent or guest molecules making them useful for adsorption and separations [22,23]. MOFs have been studied for other applications including catalysis [24] drug delivery [25,26] and chemical sensing [27,28]. MOF based chemical sensors rely on electrical, photophysical, or mechanical changes due to adsorption or reaction with an analyte [29]. MOFs used as optical sensors usually contain a fluorescent moiety such as the organic linker, metal nodes, or charge transfer between ligand and metal. Luminescence can also be generated from the interaction or absorption of guest molecules in the MOF's pores [30–32].

Rutgers Recyclable Porous Material-3 ($Zn_2(bpdc)_2(bpee)$ or RPM3) has fluorescent properties that make it attractive as a chemical sensor. A schematic representation of the 3D arrangement of Zn^{2+} metal centers between two coordinating ligands, 4,4′-biphenyldicarboxylate (bpdc) and 1,2-bipyridylethylene (bpee) of RPM3 is shown in Fig. 1 [33,34]. The conjugated linkers of RPM3 give rise to luminescence. RPM3 has been reported to detect explosive vapors such as nitrobenzene (NB), dinitrotoluene (DNT), and 2,3-dimethyl-2,3-dinitrobutane (DMNB) based on quenching of the fluorescence [34].

RPM3 also exhibits interesting sorption behavior. Stepwise hysteresis was observed for N_2 and Ar isotherms indicating the occurrence of a "gate opening" effect (GO) which was attributed to reversible structural changes occurring due to adsorption [35]. These structural changes were verified by X-ray diffraction (XRD) where the unit cell of RPM3 changes reversibly upon the removal of solvent molecules (activation) [33–36]. It has also been reported that RPM3 undergoes structural rearrangements during the adsorption of small hydrocarbons (C_1-C_4) at room temperature. The hydrocarbon adsorption–desorption isotherms exhibit GO behavior induced by formation of H-bonds between the hydrocarbon and the framework. The mechanism by which the separation of the hydrocarbons based on their chain length was recently investigated and was found to be strongly dependent on H-bond strength [37]. Although RPM3 readily adsorbs hydrocarbons, the discrimination of olefins and paraffins is more challenging. We propose that RPM3 could be functionalized with Ag^+ ions by coordination to the π bonds in the linkers. The supported Ag^+ could then be used to bind small olefins. If the Ag^+ forms a bond with the fluorescent conjugated linkers, then the fluorescence maybe modulated and sensitized to olefin bonding. The bpee linker contains a C=C bond that can form a π-complex with silver as suggested by the Chatt–Duncanson model [38]. The model describes a mechanism involving σ-donor and π-acceptor interactions between a metal ion and an olefin. The C=C of the bpee linker donates its π-bond electrons to the empty s orbital of the Ag^+, followed by the back-donation of electrons from the Ag^+ d-orbitals to the empty π^* orbitals of the C=C, as shown in Fig. 2 [38–41]. The π-complex formed between the Ag^+ and the C=C of the bpee linker of RPM3 may also bind adsorbed olefin guest molecules.

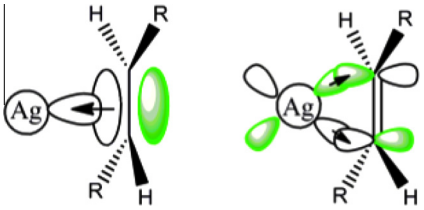

Fig. 2. Schematic representation of the interaction between the transition metal Ag^+ and an olefin. The C=C bond of the bpee linker donates its electrons to the empty s orbital of the Ag^+ (left), followed by the back-donation of electrons from the Ag^+ d-orbitals to empty π^* orbitals of the C=C (right).

In this study, RPM3 was synthesized and functionalized with $AgNO_3$ resulting in a π-complex with the conjugated bpee linker molecules monitored by Raman spectroscopy. We also demonstrated the selective, reversible detection of olefin molecules, ethylene (C_2H_4) and 1-hexene (C_6H_{12}), by Ag-RPM3 using fluorescence spectroscopy. These findings hold promise for RPM3 to be used as a chemical sensor for the reversible detection of olefins, and for olefin/paraffin separations.

2. Experimental

2.1. Materials

The following chemicals were purchased from Sigma–Aldrich. Zinc nitrate hexahydrate ($Zn(NO_3)_2.6H_2O$) CAS No. 10196-18-6,

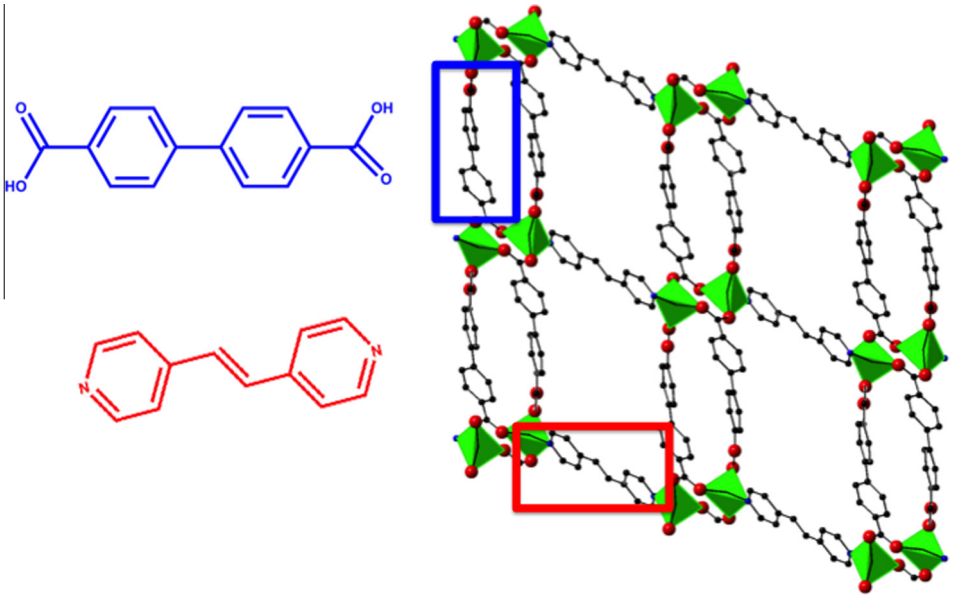

Fig. 1. RPM3 linkers (left), contains H_2bpdc (Biphenyl-4,4′-dicarboxylic acid) and bpee (1,2-Di(4-pyridyl)-ethylene). RPM3 overall structure (right) oriented in the b direction (010) obtained from reported crystallographic parameters[32].

Biphenyl-4,4′-dicarboxylic acid (H_2bpdc) (97% purity) CAS No. 787-70-2, 1,2-di(4-pyridyl)-ethylene (bpee) (97% purity) CAS No. 13362-78-2, silver nitrate $AgNO_3$ (99.9999% purity) CAS No. 7761-88-8. N,N-dimethylformamide (DMF, ACS grade) CAS No. 68-12-2, methylene chloride (CH_2Cl_2, HPLC grade) CAS No. 75-09-2, hexanes (C_6H_{14}, 55% purity) CAS No. 110-53-3, and n-heptane (C_7H_{16}, HPLC grade) CAS No. 142-82-5 were purchased from Fischer Scientific. 1-hexene (C_6H_{12}, 97% purity) CAS No. 592-41-6 was purchased from Acros Organics. Methanol (CH_3OH, ACS grade) CAS No. 67-56-1 was purchased from VWR. N_2, Ar, and C_2H_4 gas (ultra-high purity research grade) was purchased from Airgas.

2.2. Synthesis of RPM3 and solvent exchange

Briefly, $[Zn_2(bpdc)_2(bpee)]\cdot 2DMF$ (RPM3) was synthesized using a mixture of $Zn(NO_3)_2\cdot 6H_2O$, H_2bpdc, and bpee (1:1:1 M ratio) in 15 ml of DMF reacted at 165 °C for 3 days in an autoclave [34]. The RPM3 powder was activated by soaking in a solution of CH_3OH for 3 days followed by CH_2Cl_2 for 4 days, then heating at 120 °C under vacuum overnight. In order to recover as synthesized RPM, DMF was introduced into activated RPM3 via vapor deposition (VD). The method of VD involves heating activated RPM3 (~0.1 g) in a covered glass beaker with 5 ml of DMF to 80 °C for 30 min. The DMF vapor saturates the MOF's pores without suspending the MOF in solution. Following this, RPM3 can be activated again by repeating the solvent exchange method, followed by heating at 120°C under a vacuum for 24 h.

2.3. Functionalization of RPM3 (Ag-RPM3)

Silver functionalization of RPM3 powder was achieved by stirring an activated sample in a 0.01 M $AgNO_3$/DMF solution for 2 days, followed by washing the powder with CH_2Cl_2 and drying under vacuum for 24 h at 120 °C.

2.4. Characterization

XRD patterns of all samples were collected on a Rigaku Ultima IV X-ray diffractometer using a Cu Kα (λ = 1.54 Å). All patterns were collected using a 2θ range of 5–40°, and at the scan rate of 1°/min.

The morphology of all samples was determined using a SEM (Leo 1530 VP field emission scanning electron microscope). Samples were prepared for SEM by coating with Au/Pd.

Fluorescence measurements were performed on the Perkin Elmer LS 55 Luminescence Spectrometer. Solid-state fluorescence spectra were obtained using RPM3 powder and or Ag-RPM3 powder. For 1-hexene detection, fluorescence measurements were completed using activated RPM3 powder and Ag-RPM3 powder mounted on carbon sticky tape on a quartz slide. Using the front face accessory all corresponding measurements were obtained in air at room temperature. Fluorescence studies of ethylene adsorption on RPM3 and Ag-RPM3 powder was conducted using a quartz semi-micro fluorometer cell, equipped with a septum for gas introduction, purchased from Starna Cells Inc. The cycling experiments were conducted by purging the cell with the intended olefin or N_2 gas for 10 min, followed by sealing the gas within the cell. All spectral response of detection system was smoothed by adjacent averaging.

Raman spectra were collected using a micro Raman spectrometer purchased from ThermoFischer Scientific with a 780 nm solid-state laser (power = 2 mW) with a laser intensity of 5.15 mW. RPM3 and Ag-RPM3 powder samples were heated to 120 °C under N_2 within an FT-IR-600 Linkham cooling/heating Raman cell for 5 h.

Elemental analysis of Ag-RPM3 was completed by Galbraith Laboratories, Inc. Ag 9.43 wt.%, C 53.49 wt.%, H 2.94 wt.%, N 3.36 wt.%, 12.9 wt.%.

3. Results and discussion

3.1. Rpm3

3.1.1. Physical characteristics

RPM3 has a 3D microporous structure with 1D parallelogram shaped channels, and a pore window of approximately 5 × 7 Å as shown in Fig. 1 [33]. RPM3 is beige in color and is luminescent appearing bright blue ($\lambda_{emsision}$ = 420 nm) under UV irradiation (254 nm), as shown in Fig. 3.

The SEM image of RPM3 crystals exhibit a shard-like morphology, approximately 30 μm in size, see Fig. S1. The as synthesized RPM3 MOF exhibits the expected XRD pattern as shown in Fig. S2.

The RPM3 framework is very flexible, and reversible structural transformations have been reported [33]. Monitored by XRD, the as synthesized RPM3 pattern changes upon activation (solvent removal) as shown in the 3D representation in Fig. 4, pattern a. The exact structure of activated RPM3 is unknown but the shift to higher angle for the first reflection suggests a smaller unit cell [33–36,42]. The changes in structure are reversible as evident by the regeneration of as synthesized RPM3 XRD pattern, (Fig. 4, pattern b) upon re-adsorption of DMF. Fig. 4 only shows two cycles but this "breathing effect" is reversible and can be continuously repeated.

3.1.2. Characterization using Raman Spectroscopy

Insitu-Raman Spectroscopy measurements were performed to follow the change of RPM3 upon activation. Changes are observed within the fundamental modes of RPM3 upon activation as shown in Fig. 5. The 1616 cm^{-1} stretch mode is attributed to the uncoordinated C=O stretch mode that is H-bonded to the CH groups of the DMF. Upon activation this bond blue shifts to 1651 cm^{-1} as a result of DMF removal [36]. An approximate 4 cm^{-1} blue shift of the bpdc linker ν(C–O) bond stretch mode at 1621–1625 cm^{-1} was also observed, indicating a rearrangement of the bpdc linker, consistent with the structural rearrangement as observed by the XRD.

3.1.3. Characterization using fluorescence spectroscopy

It has been reported that activated RPM3 powder exhibits reversible fluorescence quenching when impregnated with electron rich solvents [33,34]. RPM3 also has a large optical band gap (3.1 eV) and it has been proposed that in the excited state, RPM3 is very reductive [34]. The large band gap and corresponding higher energy conduction band result in exceptional quenching by guest molecules [43]. Therefore the change in fluorescnce of RPM3 has the potential to be used for chemical sensing.

Activated RPM3 exhibits a fluorescence emission maximum ($\lambda_{emission}$) at approximately 420 nm when excited at 320 nm [33]. Without the presence of an inert gas such as N_2, we discovered that the fluorescence $\lambda_{emission}$ red shifts to approximately 447 nm under ambient conditions. The solid state fluorescence spectrum of as synthesized RPM3 is shown in Fig. S3. Under 40% humidity the

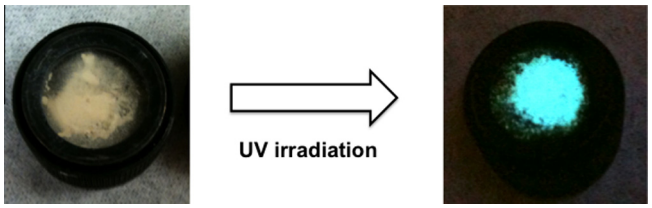

Fig. 3. Optical image of activated RPM3 (left), and activated RPM3 under UV irradiation at 254 nm (right).

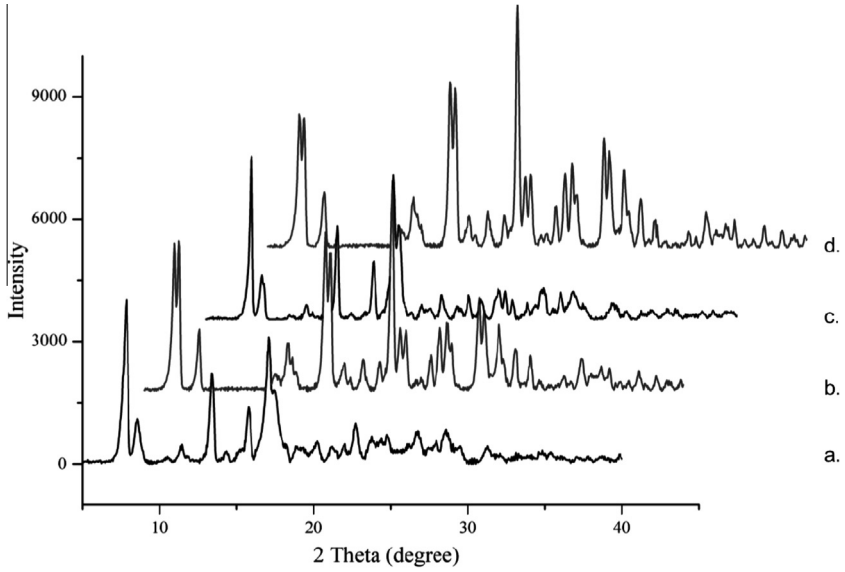

Fig. 4. A 3D representation of the XRD patterns of RPM3 activated (a), introduction of DMF (b), second activation (c), and second DMF introduction (d).

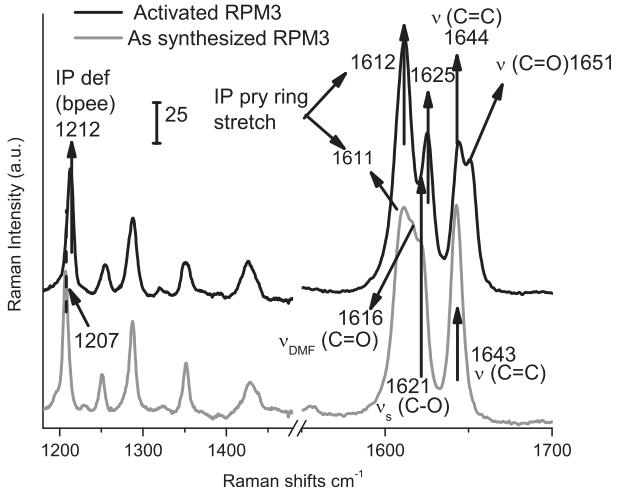

Fig. 5. Raman spectra of as synthesized (bottom grey spectrum), and activated RPM3 (top black spectrum) under N_2 at room temperature.

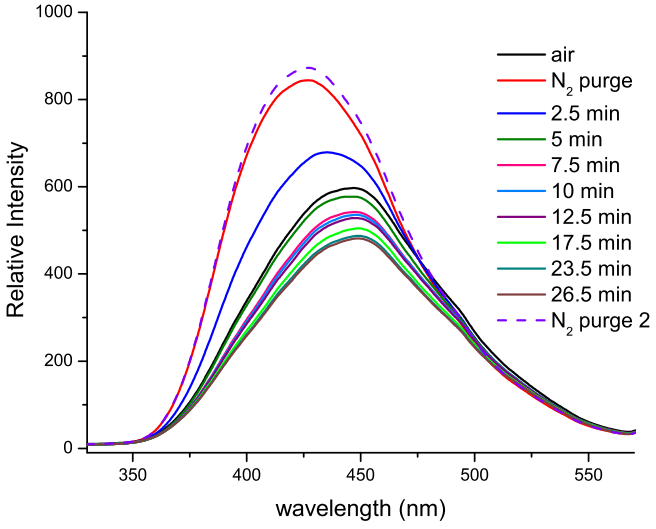

Fig. 6. Fluorescence spectra of activated RPM3 when excited at 320 nm at 40% humidity. In air (black spectrum), purged with N_2 (red spectrum), air exposure for 2.5 min (blue spectrum), increased air exposure continued for a total of 26.5 min (green through brown spectrum), purged with N_2 a second time (dotted violet spectrum). (For interpretation of color in Fig. 6, the reader is referred to the web version of this article.)

$\lambda_{emission}$ is 447 nm (black spectrum). When the system is purged with N_2 the $\lambda_{emission}$ does not change, however the signal intensity increases slightly (~9%, grey spectrum). Upon exposure to 40% humidity the fluorescence signal intensity returned (dashed black spectrum). Therefore it appears the as synthesized RPM3 fluorescence is partially quenched by moisture. The solvent free activated RPM3 fluorescence spectra as shown in Fig. 6 exhibits a $\lambda_{emission}$ = 447 nm under 40% humidity. Upon purging with N_2 the fluorescence $\lambda_{emission}$ blue shifts to 424 nm and the signal intensity increased by ~30%. The red shift and partial quenching of the fluorescence is comparable to the quenching reported for the adsorption of electron rich solvents in RPM3 [33,34]. Under ambient conditions (40% humidity) it took ~26 min to reach the maximum quenching of 43% as shown in Fig. 6. This partial quenching by moisture is completely reversible as shown by purging with N_2 (Fig. 6, dotted violet line).

3.1.4. Adsorption of olefins

The fluorescence of activated RPM3 has been determined to be quenched by moisture and solvents such as DMF. Activated RPM3 also exhibits similar results upon adsorption of olefins (Fig. S4). The fluorescence spectra of activated RPM3 purged with N_2 exhibits a band at $\lambda_{emission}$ = 424 nm (grey spectrum), which red shifts to 447 nm upon exposure to 100 ppm ethylene (black spectrum) similar to the as synthesized RPM3 and activated RPM3 in air. Along with the red shift, the $\lambda_{emission}$ signal is quenched by ~23%. These changes are reversibe; by purging with N_2 the signal intensity returns and the $\lambda_{emission}$ returns to 424 nm (dashed black spectrum). Therefore we can conclude that activated RPM3 reponds to low concentrations of gaseous olefins, showing a distinct red shift and a fluoresence quenching attributed to a proposed energy degrading mechanism as a result of the energy exchange between RPM3's conjugated linkers and the electron rich olefin molecules [44,45].

Although RPM3's fluorescence changes upon olefin adsorption do not reflect any structural transformations, a previous study postulates that activated RPM3 undergoes structural rearrangements

in the presence of introduced hydrocarbons. Guests such as ethylene and acetlyene induce rearrangements as monitored by Raman spectroscopy, as well as the liquid olefin 1-hexene as determined by XRD. Activated RPM3 under the influence of 1-hexene produces a new XRD pattern (pattern b), as shown in Fig. S5. The new 1-hexene RPM3 structure is stable under atmospheric conditions, and has been estimated to have a larger unit cell as compared to the activated RPM3, as described by *Nijem* et al. [37]. From this, we performed a detailed investigation of the activated RPM3 structure, and determined that the as synthesized RPM3 structure can be recovered no matter what guest is residing within the pores. For example, substituting the 1-hexene guest with DMF molecules generates the as synthesized pattern (Fig. S5, pattern c). Following this the activated RPM3 XRD pattern was regenerated again to demonstrate the MOF's flexibility (Fig. S5, pattern d). We then studied the fluorescence emission spectrum for 1-hexene impregnated RPM3. Fig. S6 shows activated RPM3 in air at 45% humidity with a $\lambda_{emission}$ = 447 nm (black spectrum) followed by VD of 1-hexene inducing a signal quench of less than 10%. The fluoresence change observed is similar to the changes induced from ethylene. Therefore, we can conclude that activated RPM3 exposed to an olefin has a different structure than when activated.

3.2. Ag functionalized RPM3 (Ag-RPM3)

3.2.1. Physical characteristics

The fluorescence quenching of RPM3 could be the basis for a chemical sensor. However, it does not seem to matter what guest is adsorbed (water, DMF solvent, hydrocarbons), they all seem to quench the fluorescence to varying degrees. In order to impart some selectivity for certain olefins, the RPM3 framework was functionalized with Ag^+ ions. These silver ions are expected to bind to the bpee linker in RPM3 and in turn bind olefins. Activated RPM3 was stirred in a 0.01 M $AgNO_3$ DMF solution generating Ag-RPM3. The substituted MOF was a slightly darker sandy color as compared to RPM3 before functionalization. No changes in crystallinity were observed upon functionalization based on XRD (Fig. 7, pattern b); however, some peak intensities vary as compared to the activated RPM3 pattern. Activated, un-functionalized RPM3 was not indexed; therefore we are unable to determine peak intensity correspondence. The lack of a structural change demonstrated by XRD may be due to the relatively weak nature of the Ag^+ to linker interaction. It has been reported that a Ag-olefinic bond such as Ag-C=C without the influence of auxiliary ligands on the metal has a BDE of 33.7 kcal/mol [38,40] which is considered to be weak in comparison to other transition metals able to form π-complexation bonds such as Cu and Au [46].

In order to determine the amount of Ag^+ ions present after functionalization, elemental analysis was obtained, provided by Galbraith Laboratories. Ag-RPM3 contains 9.43 wt.% Ag^+. As compared to Zn (12.90 wt.%), with 2 ions per unit cell [33], one unit cell was calculated to have 2 Ag^+ ions.

3.2.2. Characterization using Raman Spectroscopy

The *insitu*-Raman spectra in Fig. 8 show the activated RPM3 (grey spectrum) as compared to activated Ag-RPM3 (black spectrum) under N_2 atmosphere at room temperature. The Raman spectra indicate that the Ag^+ ions affect both the bpee and bpdc linkers. Changes in the Raman vibrational modes of the bpdc linker in the presence of Ag^+ ions are observed. A decrease in intensity for the C=O bond stretch mode at 1651 cm^{-1} is observed in Fig. 8a. The signal decrease is a result of a change in relative orientation of the uncoordinated C=O bond of the bpdc linker [36]. Other changes observed are a slight red shift of ~3 cm^{-1} of the moderate C–O stretch mode from 1625 to 1623 cm^{-1} shown in Fig. 8a, and a ~10 cm^{-1} blue shift of symmetric C–O stretch from 1352 to

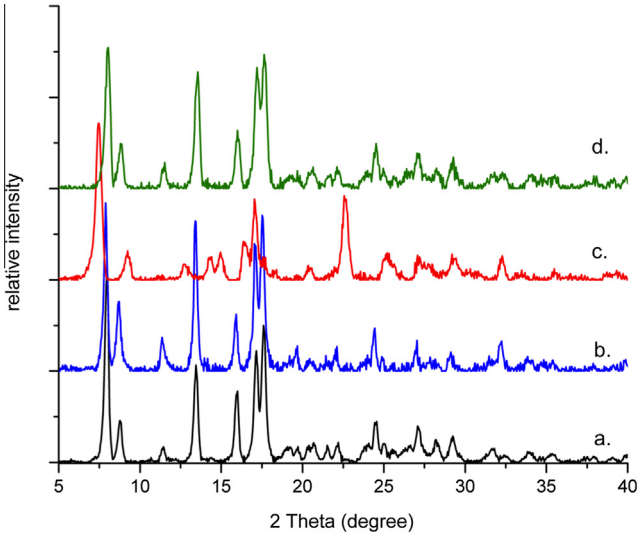

Fig. 7. XRD representation of activated RPM3 (a), activated Ag-RPM3 (b), 1-hexene solvation of Ag-RPM3 (c), and solvent free activated Ag-RPM3 after removal of 1-hexene (d).

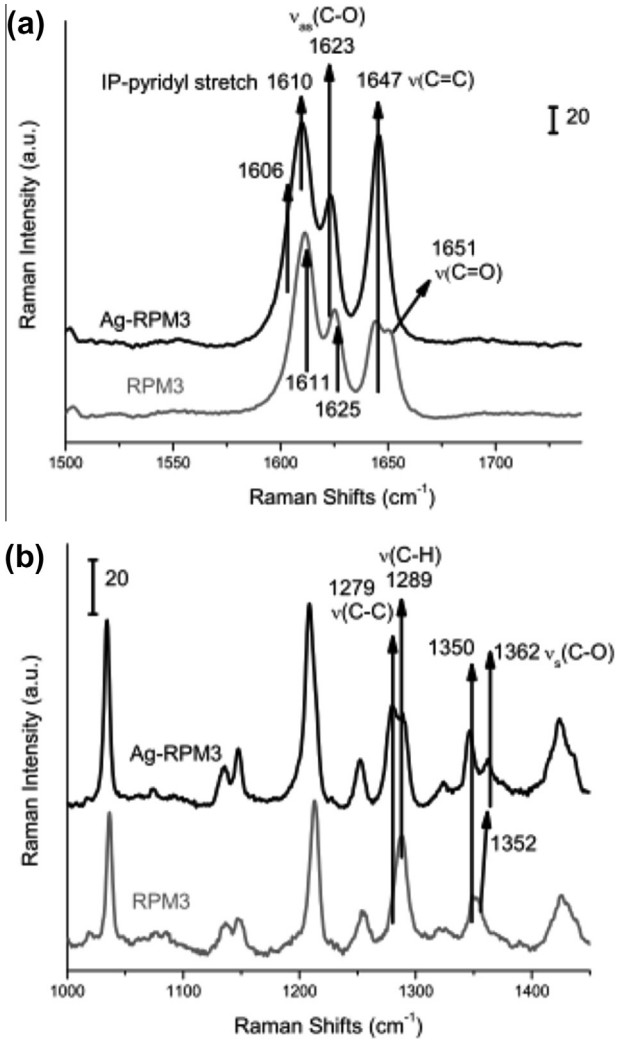

Fig. 8. Raman spectra shifts of activated RPM3 (bottom grey spectrum) compared to the activated Ag-RPM3 (top black spectrum) under N_2 purge. A scale bar of 20 is given to interpret peak intensity for both panels. Spectra range 1500–1800 cm^{-1} (a) and 1000–1450 cm^{-1} (b).

1362 cm^{-1} shown in Fig. 8b. These observations indicate a change around the Zn in the RPM3 structural building unit (SBU). An increase in intensity for the bpdc C–C stretch mode at 1279 cm^{-1} (Fig. 8b) for Ag-RPM3 occurs as a result of a change in angle between the two benzene rings. Changes related to the bpee linker include a ~3 cm^{-1} blue shift and increase in intensity for the C=C mode from 1644 to 1647 cm^{-1} (Fig. 8a) indicating an increase in polarization from Ag^+. The blue shift indicates a shortening of the C=C bond of the bpee linker, a consequence of the presence of Ag^+ ions forming a π-complex with the C=C as described by the Dewar–Chatt Duncanson model [40]. We postulate that RPM3 forms a Ag-(C=C) π-complex with the T-shaped structure dominated by σ-donation between the C=C to Ag^+ (Fig. 2, left panel) and not the common metallacyclopropane ring structure dominated by π-back donation (Fig. 2, right panel) which lengthens the C=C bond denoted by Dias *et al.* [38,47]. The lack of secondary ligands on Ag^+ affect the bonding contributions between the Ag-olefin, and C=C of the linker, leading to less π-back bonding contribution [38,47]. Ag^+ salts have been reported to exhibit weak π-back donation character in comparison to other transition metals able to form π-complex bonds such as Cu^+ [39]. Although, Cu^+ may form a stronger interaction with C=C, from the increased π-back donation, Cu^+ is not preferred for olefin detection because it is easily oxidized. The Raman spectra also shows the appearance of a shoulder at 1606 cm^{-1} (Fig. 8a) assigned to the pyridine in-plane stretch mode of the bpee linker as a result of the Ag^+ in the vicinity of the C=C bond. *In-situ* Raman spectroscopic measurements after N_2 adsorption as a function of temperature were also completed and are shown in Fig. S7. Changes to the vibrational modes from 1600 to 1660 cm^{-1} are observed at 10 °C, which is 110 °C higher than previously observed for activated RPM3 [36]. We postulate that the N_2 interaction is stronger with the Ag-RPM3 framework than with the un-functionalized RPM3 framework allowing for ease of N_2 adsorption at the higher temperature. The effect of strong N_2 adsorption is also observed for silver exchanged zeolites, in which the Ag^+ binds to N_2 through the π-complex mechanism as described by the Chatt Duncanson model [48,49].

3.2.3. Characterization using fluorescence spectroscopy

The Ag^+ ion is a common fluorescent quencher that has been used for chemical sensing applications, specifically for ratiometric fluorescent sensors [50]. Not surprisingly, activated RPM3's fluorescence ($\lambda_{emission}$ = 447 nm) is quenched upon addition of Ag^+ as shown in Fig. S8. The solid-state fluorescence measurements recorded under ambient conditions (40% humidity) shows the fluorescence emission from Ag-RPM3 unactivated to be quenched by 58% (dashed line). Activation of Ag-RPM3 at 120 °C for 12 h; enhanced the fluorescence by 33% (dotted line). The fluorescence enhancement due to activation is expected because DMF slightly quenches the RPM3's fluorescence [33,34]. Overall the fluorescence signal ($\lambda_{emission}$ = 447 nm) was quenched by 45% with the addition of Ag^+ ion.

The activated Ag-RPM3 also exhibits the same red shift and fluorescence quenching when exposed to moisture as the activated RPM3. Fig. 9 shows the fluorescence spectra for Ag-RPM3 in air at 45% humidity has a $\lambda_{emission}$ = 447 nm (black spectrum), and after purging with N_2 the $\lambda_{emission}$ blue shifts to 424 nm with an intensity enhancement of 25% (red spectrum). This Figure also shows the Ag-RPM3 fluorescence shift and quenching as a function of time. Activated RPM3 exceeded the initial fluorescence signal intensity in air after 5 min; however, Ag-RPM3 does not exceed its original intensity until 12.5 min and at 5% higher humidity. We monitored Ag-RPM3 for 50 min after which the quenching did not change; therefore, Ag-RPM3 was quenched overall by 35%. The activated RPM3 fluorescence was quenched 43% over a time period of 26 min, as described in Section 3.1.3. The Ag-RPM3 appears to be less sensitive to moisture.

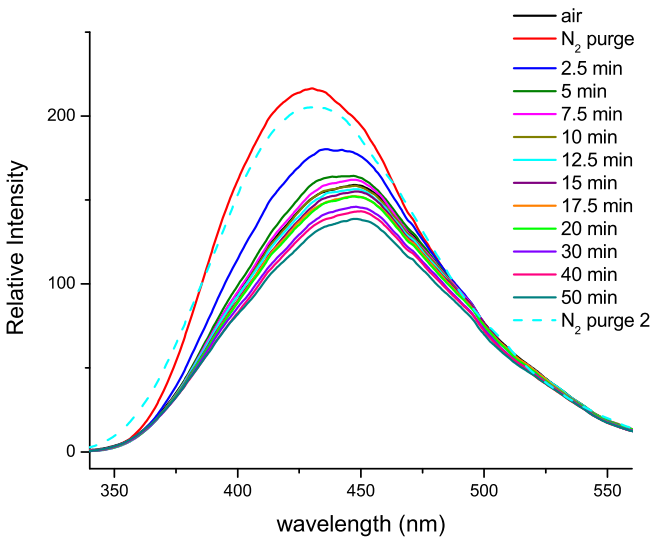

Fig. 9. Fluorescence spectra at room temperature, 45% humidity, of activated Ag-RPM3 when excited at 320 nm. In air (black spectrum), purged with N_2 (red spectrum), 2.5 min atmosphere exposure (blue spectrum), increased atmosphere exposure continued for a total of 50 min (cyan spectrum through orange spectrum, second N_2 purge (dotted light blue spectrum). (For interpretation of color in Fig. 9, the reader is referred to the web version of this article.)

3.2.4. Adsorption of olefins

We have demonstrated that the fluoresence spectra of activated RPM3 red shifts in the presence of olefins such as ethylene, and 1-hexene, as described in Section 3.1.4. Structural changes occur during olefin adsoprtion as observed by XRD (shown in Fig. S5). Therefore, activated RPM3 is not a promising canidate for olefin detection or olefin/paraffin separations because the changes are not selective or distinguishable under atmospheric conditions.

Ag-RPM3 responds to olefin molecules differently. A fluorescence enhancement is observed upon the addition of ethylene, and 1-hexene. Fluorescence enhancement is a common phenomenom encountered for MOF's upon the addition of analytes with electron donating groups. MOFs containing d^{10} metals and highly conjugated linkers have extended networks with narrow band gaps. Upon excitation, a MOF in the presence of an analyte with electron donating groups go through an electron transfer phenomenom. The analyte's electrons are transferred from the LUMO to the MOF's lower conduction band (CB), resulting in fluorecence enhancement [51,52]. Using the quartz semi-micro fluorometer cell, ethylene was introduced into Ag-RPM3. The Ag-RPM3 fluorescence emission at $\lambda_{emission}$ = 424 nm is enhanced by 42% upon exposure to 100 ppm ethylene, as shown in Fig. 10, dashed spectrum. The $\lambda_{emission}$ signal returns when purged with N_2 for 30 min (dotted spectrum). This intensity change is reversible as shown in Fig. 11.

In the presence of 1-hexene, a fluorescence enhancement is also observed as shown in Fig. 12. Ag-RPM3 in air exhibits a $\lambda_{emission}$ = 447 nm (black spectrum) which shifts to 424 nm with an increase in intensity of 43% upon 1-hexene introduction (top black spectrum). Heating under vacuum at 150 °C for 24 h can reverse this change (grey dotted spectrum). The stability of Ag-RPM3 was studied by cycling the 1-hexene in and out of the framework multiple times as shown in Fig. 13. From this we can conclude that Ag-RPM3 experiences a reversible fluorescence enhancement of ~42–43% for olefins such as ethylene, and 1-hexene. The results for a control fluorescence experiment using the paraffins, hexanes,

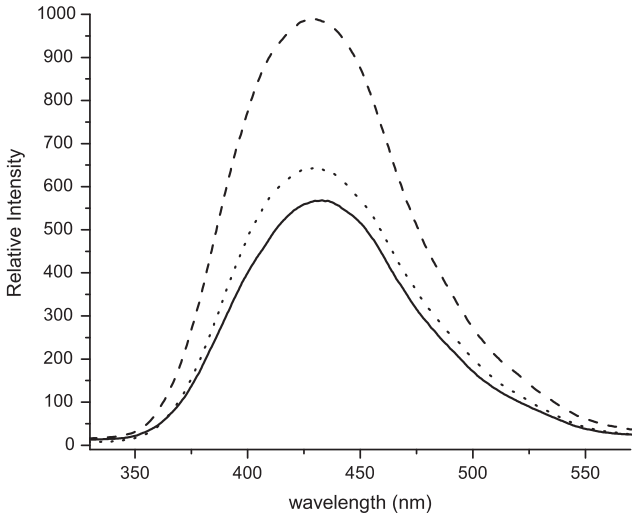

Fig. 10. Fluorescence spectra at room temperature, when excited at 320 nm of activated Ag-RPM3. Purged with N_2 (black spectrum), purged with 100 ppm C_2H_4/N_2 (dashed spectrum), second N_2 purge (dotted spectrum).

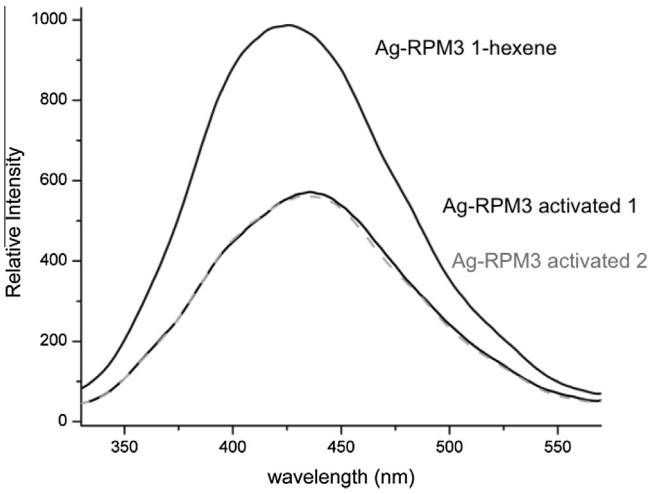

Fig. 12. Fluorescence spectra at room temperature, excited at 320 nm of activated Ag-RPM3 in air at 40% humidity (black spectrum), 1-hexene VD in air at 40% humidity (top black spectrum), 1-hexene removed in air at 40% humidity (dotted grey spectrum).

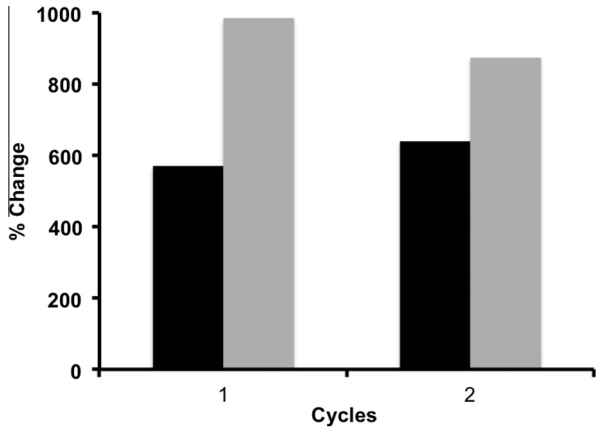

Fig. 11. Changes in intensity of Ag-RPM3 upon fluorescence cycling with N_2 and ethylene. Activated Ag-RPM3 under N_2 (left black bar), Ag-RPM3 exposed to 100 ppm C_2H_4/N_2 (right grey bar).

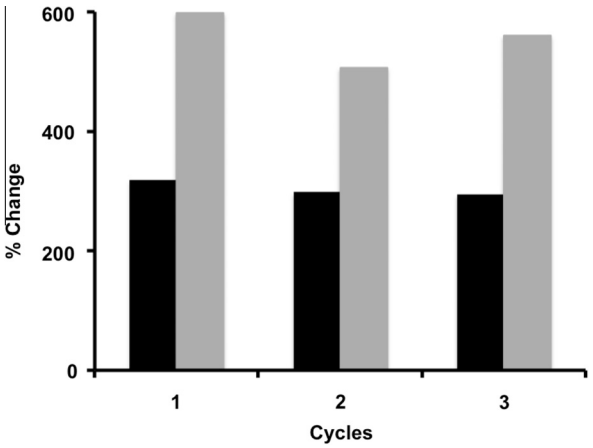

Fig. 13. Changes in intensity of Ag-RPM3 upon fluorescence cycling with N_2 and 1-hexene. Activated Ag-RPM3 under N_2 (left black bar), Ag-RPM3 impregnated with 1-hexene (right grey bar).

and n-heptane adsorbed in Ag-RPM3 is shown in Fig. S9. Paraffin adsorption resulted in no fluorescence enhancement for Ag-RPM3. Therefore, the interaction of the olefin with the Ag^+ ion is required to observe a distinguishable change.

The adsorption of 1-hexene in Ag-RPM3 results in a similar XRD change as observed for activated RPM3 (shown in Fig. 7). Ag-RPM3 exhibits a new XRD pattern when 1-hexene is introduced. The activated pattern can be regenerated by repeating the solvent exchange procedure described in Section 2.2. Previously activated RPM3 was determined to have a higher binding energy with 1-hexene than shorter chain olefins such as ethylene [37]. The Raman spectra in Fig. S10 compares activated RPM3 (bottom spectrum) against Ag-RPM3 (middle spectrum) and 1-hexene impregnated Ag-RPM3 (top spectrum). An ~6 cm^{-1} red shift is observed for the C=C bond stretch of the bpee linker when 1-hexene is adsorped into the pores of Ag-RPM3, 1647–1641 cm^{-1}. This is consistent with the binding of 1-hexene to the Ag^+ ion bound to bpee linker where a charge redistribution must occur. Changes in the ν(C–O) asymmetric stretch mode at 1625 cm^{-1} are also observed and can be attributed to structural modification of the framework after incorporation of 1-hexene. Similar changes were reported involving 1-hexene adsorption on activated RPM3 in a recent study by *Nijem* et al., however these changes were found to orginate from the structural arrangements of the framework after adsorption of the hydrocarbon [37]. Changes also occur for the symmetric C–O stretch at 1362 cm^{-1} present within Ag-RPM3's spectrum. Upon 1-hexene adsorption the C–O stretch red shifts to 1352 cm^{-1}, overlaping with the symmetric C–O stretch for activated RPM3. This change indicates that 1-hexene is interacting with the Ag^+ ions bound to the framework; without the presence of 1-hexene the C–O stretch is blue shifted due to changes occuring around the metal node as described in Section 3.2.2.

In the case of 100 ppm ethylene adsorption by Ag-RPM3 the changes in the Raman spectra are more subtle as shown in Fig. S11. A decrease in the intensity of C=C stretch of the bpee linker at 1647 cm^{-1} and the asymmetric stretch mode of the C–O stretch of the bpdc linker at 1625 cm^{-1} are observed. These changes indicate that the Ag^+ is interacting with ethylene, however, no structural rearrangement of Ag-RPM3 may occur at such a low concentration.

4. Conclusion

In this work, RPM3 was successfully functionalized with $AgNO_3$ for the selective detection of olefins. We monitored the changes

invoked upon Ag^+ functionalization using XRD, Raman and fluorescence spectroscopy. The Ag-RPM3 exhibits a fluorescence enhancement of ~42–43% upon the introduction of olefins including 1-hexene and ethylene by forming a π complex. The Ag-RPM3 exhibits selectivity for olefins over the corresponding paraffins. The Ag-RPM exhibits a strong optical response to ethylene at 100 ppm suggesting even lower concentration might be detected. These results demonstrate Ag-RPM3's potential to be used in future olefin/paraffin separations through reactive adsorption and for its use as a chemical sensor.

Acknowledgments

I would like to thank the Robert A. Welch Foundation AT1153 for funding this work, and Layne D. McBeath for his help with this project.

Appendix A. Supplementary data

Supplementary data associated with this article can be found, in the online version, at http://dx.doi.org/10.1016/j.micromeso.2013.02.044.

References

[1] T. Ren, M. Patel, K. Blok, Energy 31 (2006) 425–451.
[2] N. Rahimi, R. Karimzadeh, Appl. Catal. A 398 (2011) 1–17.
[3] A.F.P. Ferreira, J.C. Santos, M.G. Plaza, N. Lamia, J.M. Loureiro, A.E. Rodrigues, Chem. Eng. J. 167 (2011) 1–12.
[4] J. Padin, R.T. Yang, C.L. Munson, Ind. Eng. Chem. Res. 38 (1999) 3614–3621.
[5] R.T. Yang, E.S. Kikkinides, AlChE J. 41 (1995) 509–517.
[6] J.-F. Huang, H. Luo, C. Liang, D.-e. Jiang, S. Dai, Ind. Eng. Chem. Res. 47 (2008) 881–888.
[7] L.M. Galán Sánchez, G.W. Meindersma, A.B. Haan, Ind. Eng. Chem. Res. 48 (2009) 10650–10656.
[8] S.W. Kang, J.H. Kim, K.S. Oh, J. Won, K. Char, H.S. Kim, Y.S. Kang, J. Membr. Sci. 236 (2004) 163–169.
[9] K. Nymeijer, T. Visser, R. Assen, M. Wessling, J. Membr. Sci. 232 (2004) 107–114.
[10] C. Staudt-Bickel, W.J. Koros, J. Membr. Sci. 170 (2000) 205–214.
[11] G. Mothé, M. Castro, M. Sthel, G. Lima, L. Brasil, L. Campos, A. Rocha, H. Vargas, Sensors 10 (2010) 9726–9741.
[12] C. Popa, A.M. Bratu, C. Matei, R. Cernat, A. Popescu, D.C. Dumitras, Laser Phys. 21 (2011) 1336–1342.
[13] R.J. Dexter, J.C. Verdonk, B.A. Underwood, K. Shibuya, E.A. Schmelz, D.G. Clark, J. Exp. Bot. 59 (2008) 609–618.
[14] V. Kumar, G. Parvatam, G.A. Ravishankar, Electron. J. Biotechnol. 12 (2009) 1–15.
[15] P. Pattananuwat, D. Aht-ong, Mater. Sci. Forum 695 (2011) 336–339.
[16] S.M. Cristescu, D. De Martinis, S. Te Lintel Hekkert, D.H. Parker, F.J.M. Harren, Appl. Environ. Microbiol. 68 (2002) 5342–5350.
[17] C. Baratto, G. Faglia, M. Pardo, M. Vezzoli, L. Boarino, M. Maffei, S. Bossi, G. Sberveglieri, Sens. Actuators B 108 (2005) 278–284.
[18] B. Esser, J.M. Schnorr, T.M. Swager, Angew. Chem. Int. Ed. (2012) 5752–5756.
[19] A. Bétard, R.A. Fischer, Chem. Rev. 112 (2012) 1055–1083.
[20] S.T. Meek, J.A. Greathouse, M.D. Allendorf, Adv. Mater. 23 (2011) 249–267.
[21] A. Dhakshinamoorthy, M. Alvaro, A. Corma, H. Garcia, Dalton Trans. 40 (2011) 6344–6360.
[22] D.J. Collins, H.-C. Zhou, J. Mater. Chem. 17 (2007) 3154–3160.
[23] J.-R. Li, J. Sculley, H.-C. Zhou, Chem. Rev. 112 (2011) 869–932.
[24] M. Ranocchiari, J.A.v. Bokhoven, Phys. Chem. Chem. Phys. 13 (2011) 6388–6396.
[25] A.C. McKinlay, R.E. Morris, P. Horcajada, G. Férey, R. Gref, P. Couvreur, C. Serre, Angew. Chem. Int. Ed. 49 (2010) 6260–6266.
[26] R.C. Huxford, J. Della Rocca, W. Lin, Curr. Opin. Chem. Biol. 14 (2010) 262–268.
[27] B. Gole, A.K. Bar, P.S. Mukherjee, Chem. Commun. 47 (2011) 12137–12139.
[28] N.B. Shustova, B.D. McCarthy, M. Dincă, J. Am. Chem. Soc. 133 (2011) 20126–20129.
[29] L.E. Kreno, K. Leong, O.K. Farha, M. Allendorf, R.P. Van Duyne, J.T. Hupp, Chem. Rev. 112 (2012) 1105–1125.
[30] X. Zou, G. Zhu, I.J. Hewitt, F. Sun, S. Qiu, Dalton Trans. (2009).
[31] S. Liu, Z. Xiang, Z. Hu, X. Zheng, D. Cao, J. Mater. Chem. 21 (2011).
[32] R.J. Kuppler, D.J. Timmons, Q.-R. Fang, J.-R. Li, T.A. Makal, M.D. Young, D. Yuan, D. Zhao, W. Zhuang, H.-C. Zhou, Coord. Chem. Rev. 253 (2009) 3042–3066.
[33] A. Lan, K. Li, H. Wu, L. Kong, N. Nijem, D.H. Olson, T.J. Emge, Y.J. Chabal, D.C. Langreth, M. Hong, J. Li, Inorg. Chem. 48 (2009) 7165–7173.
[34] A. Lan, K. Li, H. Wu, D.H. Olson, T.J. Emge, W. Ki, M. Hong, J. Li, Angew. Chem. Int. Ed. 48 (2009) 2334–2338.
[35] S. Sircar, H. Wu, J. Li, A.D. Lueking, Langmuir 27 (2011) 14169–14179.
[36] N. Nijem, P. Thissen, Y. Yao, R.C. Longo, K. Roodenko, H. Wu, Y. Zhao, K. Cho, J. Li, D.C. Langreth, Y.J. Chabal, J. Am. Chem. Soc. 133 (2011) 12849–12857.
[37] N. Nijem, H. Wu, P. Canepa, A. Marti, K.J. Balkus, T. Thonhauser, J. Li, Y.J. Chabal, J. Am. Chem. Soc. 134 (2012) 15201–15204.
[38] H.V.R. Dias, J. Wu, Eur. J. Inorg. Chem. (2008) 509–522.
[39] R.T. Yang, Adsorbents: Fundamentals and Applications, John Wiley & Sons, Holboken, 2003.
[40] R.H. Hertwig, W. Koch, D. Schröder, H. Schwarz, J. Hrušák, P. Schwerdtfeger, J. Phys. Chem. 100 (1996) 12253–12260.
[41] Y.M. Lee, S.J. Choi, Y. Kim, K. Seff, J. Phys. Chem. B 109 (2005) 20137–20144.
[42] H. Wu, R.S. Reali, D.A. Smith, M.C. Trachtenberg, J. Li, Chem. Eur. J. 16 (2010) 13951–13954.
[43] S.W. Thomas Iii, J.P. Amara, R.E. Bjork, T.M. Swager, Chem. Commun. (2005) 4572–4574.
[44] O. Divya, A.K. Mishra, Anal. Chim. Acta 630 (2008) 47–56.
[45] Y. Xiao, L. Wang, Y. Cui, B. Chen, F. Zapata, G. Qian, J. Alloys Compd. 484 (2009) 601–604.
[46] H.Y. Huang, J. Padin, R.T. Yang, J. Phys. Chem. B 103 (1999) 3206–3212.
[47] C. Elschenbroich, Organometallics, 3rd ed., Wiley-VCH, Weinheim, 2006. pp. 399–403.
[48] A. Ansón, S.M. Kuznicki, T. Kuznicki, T. Haastrup, Y. Wang, C.C.H. Lin, J.A. Sawada, E.M. Eyring, D. Hunter, Microporous Mesoporous Mater. 109 (2008) 577–580.
[49] R.T. Yang, Y.D. Chen, J.D. Peck, N. Chen, Ind. Eng. Chem. Res. 35 (1996) 3093–3099.
[50] F. Wang, R. Nandhakumar, J.H. Moon, K.M. Kim, J.Y. Lee, J. Yoon, Inorg. Chem. 50 (2011) 2240–2245.
[51] S. Pramanik, C. Zheng, X. Zhang, T.J. Emge, J. Li, J. Am. Chem. Soc. 133 (2011) 4153–4155.
[52] Q. Zhu, C. Shen, C. Tan, T. Sheng, S. Hu, X. Wu, Chem. Commun. 48 (2012) 531–533.